



Golden Galactic Binaries for LISA: Mass-transferring White Dwarf Black Hole Binaries

Laura Sberna¹ , Alexandre Toubiana^{2,3} , and M. Coleman Miller⁴ ¹ Perimeter Institute, 31 Caroline Street N, Waterloo, ON N2L 2Y5, Canada² APC, AstroParticule et Cosmologie, Université Paris Diderot, CNRS/IN2P3, CEA/Irfu, Observatoire de Paris, Sorbonne Paris Cité, 10, rue Alice Domon et Léonie Duquet F-75205 Paris Cedex 13, France³ Institut d'Astrophysique de Paris, CNRS & Sorbonne Universités, UMR 7095, 98 bis bd Arago, F-75014 Paris, France⁴ Department of Astronomy and Joint Space-Science Institute, University of Maryland College Park, MD 20742-2421, USA

Received 2020 October 12; revised 2020 November 14; accepted 2020 November 19; published 2021 February 8

Abstract

We study the evolution and gravitational wave emission of white dwarf–black hole accreting binaries with a semianalytical model. These systems will evolve across the mHz gravitational wave frequency band and potentially be detected by the Laser Interferometer Space Antenna (LISA). We identify new universal relations for this class of binaries, which relate the component masses to the gravitational wave frequency and its first derivative. Combined with the high precision measurements possible with LISA, these relations could allow us to infer the component masses and the luminosity distance of the source. LISA has therefore the potential to detect and characterize a virtually unexplored binary population.

Unified Astronomy Thesaurus concepts: Gravitational waves (678); Accretion (14); Compact binary stars (283); White dwarf stars (1799); Astrophysical black holes (98)

1. Introduction

Galactic compact binaries will form a stochastic foreground signal that, from $\text{few} \times 10^{-4}$ Hz to $\text{few} \times 10^{-3}$ Hz, will dominate over the instrumental noise of the Laser Interferometer Space Antenna (LISA; Amaro-Seoane et al. 2017), a gravitational wave (GW) space-borne experiment scheduled for launch in 2034 (Nelemans et al. 2001c, 2001a, 2001b; Liu et al. 2010; Rüter et al. 2010; Yu & Jeffery 2010). In addition to this foreground, LISA is expected to individually resolve $\sim 10^4$ compact binaries (Nelemans et al. 2004; Kremer et al. 2017; Korol et al. 2017; Lamberts et al. 2019; Breivik et al. 2020b). Among Galactic binaries, double white dwarfs (DWDs) are predicted to be the most numerous sources. These binaries will be observed both in the mass-accreting and in the detached phase and could be targeted by other surveys in the electromagnetic band, such as Gaia (Breivik et al. 2018). The detection of such a large number and wide range of white dwarf (WD) binaries will allow the Milky Way to be mapped (Adams et al. 2012; Korol et al. 2018; Breivik et al. 2020a), to explore Milky Way satellites (Korol et al. 2020; Roebber et al. 2020), measure the influence of tidal couplings (Fuller & Lai 2012; Shah et al. 2015), test binary population models (Toonen et al. 2014), and even test general relativity (Littenberg & Yunes 2019).

Little attention has so far been devoted to another class of galactic binaries: accreting white dwarf–black hole binaries (WDBH; see, however, van Haften et al. 2012). Population studies predict that tens of thousands of mass-transferring WDBHs could form in the Milky Way (see, e.g., Hurley et al. 2002; Yungelson et al. 2006), but the rates are still uncertain by more than an order of magnitude. The expectation is that binaries containing a black hole (BH) will be subdominant in the range of frequencies relevant for LISA (0.1–1 mHz, see, e.g., Nelemans et al. 2001b). Although Breivik et al. (2020b) suggest that LISA might not see any detached WDBHs in the Galaxy, Kremer et al. (2018) find that a few events could be possible if we account for binary interactions in Galactic globular clusters. Overall, these sources are often discarded in

BH population synthesis simulations (e.g., Lamberts et al. 2018) and further investigations are needed to predict the rate of their mass-transferring phase.

There are no confirmed observations of WDBH binaries from electromagnetic surveys, although these binaries, like other mass-transferring systems, are expected to emit across a broad spectrum and have even been suggested to produce gamma-ray bursts (Dong et al. 2018). The X-ray binary X-9, in the globular cluster 47 Tucanae, might host a WD and a BH (Miller-Jones et al. 2015; Church et al. 2017; Tudor et al. 2018), but the system is also consistent with a neutron star accretor. Other candidates include XMMUJ122939.7+075333 in a globular cluster of the Virgo Galaxy NGC 4472 (Maccarone et al. 2007). LISA will thus provide a complementary investigation of this elusive population and might be the first observatory to confirm their existence.

In this article, we demonstrate that a LISA observation of a WDBH binary would reveal the component masses and the luminosity distance of the system. In Section 2, we describe our semianalytical model to evolve WDBH binaries. We then determine two universal relations followed by these binaries in their evolution: one common to binaries with a WD (Helium) donor (e.g., Nelemans 2005; Breivik et al. 2018) and one, first appearing in this work, applicable to accreting binaries with small tidal interactions. In Section 4 we use these relations to infer the WD mass M_{WD} , the BH mass M_{BH} , and the luminosity distance D_L from a LISA measurement of the GW amplitude and the frequency f and its first derivative \dot{f} .

2. Evolution of Mass-transferring WDBH Binaries

We consider WDBH binaries on a circular orbit with separation a . We model their evolution from the onset of mass transfer, when the WD overfills its Roche lobe. Our treatment follows that of Marsh et al. (2004), with appropriate adjustments for the BH component. We define the total mass $M = M_{\text{BH}} + M_{\text{WD}}$ and the mass ratio $q = M_{\text{WD}}/M_{\text{BH}} \leq 1$. We use

Eggleton’s approximation for the zero-temperature mass–radius relation (Verbunt & Rappaport 1988) of the WD⁵

$$\frac{R_{\text{WD}}}{R_{\odot}} = 0.0114 \left[\left(\frac{M_{\text{WD}}}{M_{\text{Ch}}} \right)^{-2/3} - \left(\frac{M_{\text{WD}}}{M_{\text{Ch}}} \right)^{2/3} \right]^{1/2} \times \left[1 + 3.5 \left(\frac{M_{\text{WD}}}{M_{\text{p}}} \right)^{-2/3} + \left(\frac{M_{\text{WD}}}{M_{\text{p}}} \right)^{-1} \right]^{-2/3}, \quad (1)$$

with $M_{\text{Ch}} = 1.44M_{\odot}$ and $M_{\text{p}} = 0.00057M_{\odot}$.

2.1. Mass Transfer

The overflow factor indicates by how much the donor overfills its Roche lobe, $\Delta = R_{\text{WD}} - R_L$. Mass transfer occurs when $\Delta > 0$ and increases monotonically with the overflow. We use the adiabatic approximation of Marsh et al. (2004; see also Webbink 1984):

$$\dot{M}_{\text{WD}} = -F(M_{\text{BH}}, M_{\text{WD}}, a, R_{\text{WD}})\Delta^3. \quad (2)$$

See Marsh et al. (2004) for the definition of F . We assume an accretion disk forms around the BH and that matter is transferred from the innermost stable circular orbit (ISCO) at a radius R_{ISCO} (Chandrasekhar 1984). We account for the limited efficiency of the BH to accrete by setting:

$$\dot{M}_{\text{BH}} = \min(-\dot{M}_{\text{WD}} \epsilon_{\text{ISCO}}, \dot{M}_{\text{Edd}}(M_{\text{BH}})), \quad (3)$$

where $\dot{M}_{\text{Edd}} = 2.2 \times 10^{-8} M_{\text{BH}} \text{ yr}^{-1}$ is the Eddington accretion rate and ϵ_{ISCO} is the specific mass-energy at the ISCO (Chandrasekhar 1984). Therefore mass is not necessarily conserved, accounting for possible loss through winds.

2.2. Orbital Separation

We assume that the variation of total angular momentum is due to GW emission and loss of matter:

$$\dot{J}_{\text{orb}} + \dot{J}_{\text{BH}} + \dot{J}_{\text{WD}} = -\dot{J}_{\text{GW}} - \dot{J}_{\text{loss}}, \quad (4)$$

with $\dot{J}_{\text{GW}} = \frac{32}{5} \frac{G^3 M_{\text{BH}} M_{\text{WD}} M}{c^5 a^4} J_{\text{orb}}$. Following van Haften et al. (2012), we assume isotropic re-emission and take $\dot{J}_{\text{loss}} = -q \frac{\dot{M}}{M} J_{\text{orb}}$. We neglect the angular momentum of the accretion disk surrounding the BH, assuming that $M_{\text{disk}} \ll M_{\text{BH}}$ throughout the evolution.

We assume that the WD is tidally locked. This is justified in low-mass-ratio systems such as WDBH binaries, since the synchronization timescale decreases as the mass ratio squared, $\tau_{\text{sync}} \sim q^2$ (Campbell 1984). Moreover, disk accretion can also contribute to synchronizing the star rotation with the orbit (Zahn 1977). The angular momentum of the donor can then be written as $J_{\text{WD}} = I_{\text{WD}} \Omega$, Ω being the orbital angular frequency and $I_{\text{WD}} = k M_{\text{WD}} R_{\text{WD}}^2$ the momentum of inertia of the donor. The factor k is a function of the WD mass, for which we use the fit provided in Marsh et al. (2004). Using Kepler’s

law, the variation in angular momentum of the donor is:

$$\dot{J}_{\text{WD}} = I_{\text{WD}} \Omega \left(\lambda \frac{\dot{M}_{\text{WD}}}{M_{\text{WD}}} - \frac{3}{2} \frac{\dot{a}}{a} + \frac{\dot{M}_{\text{BH}} + \dot{M}_{\text{WD}}}{M_{\text{WD}}} \frac{1}{2(1+1/q)} \right), \quad (5)$$

where $\lambda = 1 + 2 \frac{d \log R_{\text{WD}}}{d \log M_{\text{WD}}} + \frac{d \log k}{d \log M_{\text{WD}}}$. Note that the variation of the donor angular momentum was not included in the treatment of Marsh et al. (2004).

We assume no tidal torque acts on the BH, so its angular momentum varies only as a result of the matter accreted at R_{ISCO} ,

$$\dot{J}_{\text{BH}} = j_{\text{ISCO}} \dot{M}_{\text{BH}}, \quad (6)$$

where j_{ISCO} is the specific angular momentum at the ISCO (Chandrasekhar 1984). In Appendix A we derive the resulting equation for the binary separation as a function of time.

2.3. Overflow and Black Hole Spin

We evolve the overflow factor according to

$$\dot{\Delta} = R_{\text{WD}} \left[(\zeta_{\text{WD}} - \zeta_{r_L}) \frac{\dot{M}_{\text{WD}}}{M_{\text{WD}}} - \frac{\dot{a}}{a} \right], \quad (7)$$

where $\zeta_{\text{WD}} = \frac{d \log R_{\text{WD}}}{d \log M_{\text{WD}}}$ and $\zeta_{r_L} = \frac{d \log R_L / a}{d \log M_{\text{WD}}}$ can be derived using Eggleton’s approximation for the mass–radius relationship of cold WDs (Equation (1)) and Eggleton’s Roche lobe fitting formula (Eggleton 1983), respectively. The latter reads:

$$R_L = \frac{0.49}{0.6 + q^{2/3} \ln(1 + q^{-1/3})} a. \quad (8)$$

Note that our definition of the mass ratio q is inverted with respect to Eggleton (1983), thus the difference in Equation (8).

The angular momentum of the BH can be written in terms of the dimensionless spin χ ,

$$J_{\text{BH}} = \frac{G}{c} M_{\text{BH}}^2 \chi. \quad (9)$$

The accreting BH will spin up according to Equation (6), from which we obtain

$$\dot{\chi} = \left(\frac{c}{G} \frac{j_{\text{ISCO}}}{M_{\text{BH}}} - 2\chi \right) \frac{\dot{M}_{\text{BH}}}{M_{\text{BH}}}. \quad (10)$$

The evolution of the BH spin is not our main focus and has little effect on the overall evolution of the binary. We therefore neglect for simplicity other factors affecting the spin evolution, such as radiation emitted by the accretion disk and fix the initial BH spin to $\chi = 0.1$.

2.4. Results

We numerically integrate Equations (2), (3), (4), (7), and (10), starting from the onset of mass transfer. The long-term evolution of a typical WDBH binary is shown in Figure 1. The cap in the BH accretion rate on the top panel is due to accretion reaching the Eddington limit. As expected for mass-transfer-dominated systems where the accretor is much more massive than the donor, the binary outspiral, giving a negative \dot{f} .

⁵ Note that the accretion disk surrounding the BH can heat the WD. We will discuss this caveat further in the conclusions.

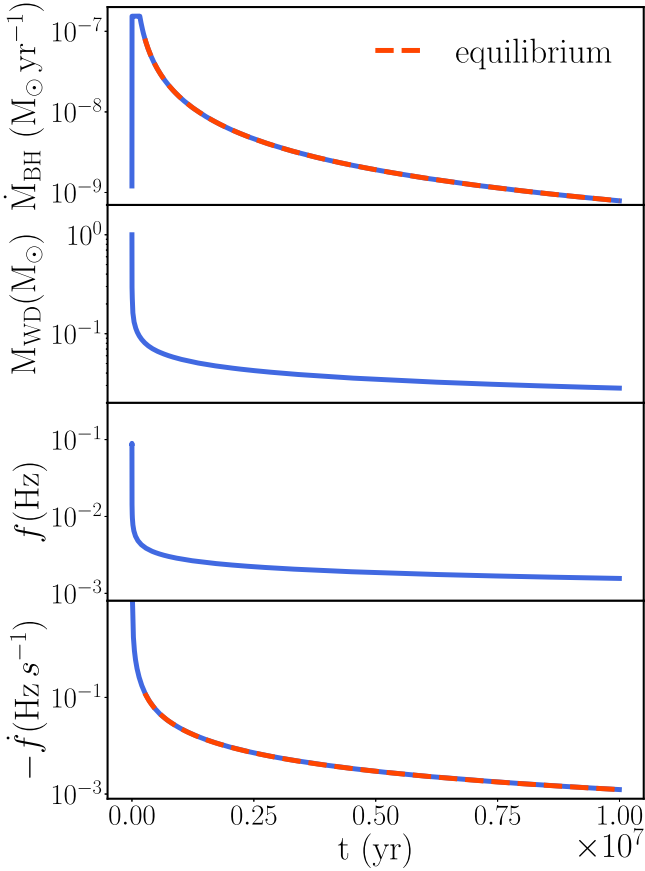


Figure 1. Evolution of the mass accretion rate, WD mass, GW frequency, and its first derivative. The system has masses $M_{\text{WD}} = 1 M_{\odot}$ and $M_{\text{BH}} = 7 M_{\odot}$ at the time of first Roche lobe filling. The overlaid orange dashed line is the equilibrium solution described in Appendix B.

Mass transfer proceeds rapidly at first, but quickly settles into an equilibrium rate. Equilibrium is attained when the increase in the Roche lobe matches the one in the WD radius. Thus, we obtain the equilibrium mass transfer rate by setting the right-hand side (rhs) of Equation (7) to 0, see Appendix B.

3. Universal Relations

Across parameter space, the mass of the WD follows an evolutionary track as a function of the GW frequency, which is approximately independent of the accretor mass and the initial conditions, as displayed in Figure 2, left panel. We span initial WD masses between $[0.2, 1.2] M_{\odot}$, initial BH masses in the range $[3, 20] M_{\odot}$, and only keep points from the equilibrium stage. These tracks can be compared with the ones traced by WD accreting binaries in Breivik et al. (2018). Our WDBH tracks follow a slightly different trajectory and show a more pronounced dependence on the accretor mass, resulting in a larger spread in the tracks (and hence fit residuals).

The absence of tidal torques acting on the WD and the BH yields an additional relation between $\dot{f} M_{\text{BH}}^{-2/3}$ and f . We show this relation in Figure 2, right panel. Once again, the relation is roughly independent of the accretor mass and initial conditions. In Appendix B we explain how this relation can be derived from the equilibrium solution.

We fit both evolutionary track relations with a quartic polynomial $\log(y) = \sum_{i=0}^n a_i \log(f [\text{Hz}])^i$ (Figure 2). The fit coefficients are listed in Appendix C.

4. Parameter Estimation with LISA

In the case of almost monochromatic sources such as WDBH and double WD binaries, the two GW polarizations take the simple form:

$$h_+ = A_0 \frac{1}{2} (1 + \cos^2(\iota)) \cos(\phi_0 + 2\pi f t + \pi \dot{f} t^2),$$

$$h_{\times} = A_0 \cos(\iota) \sin(\phi_0 + 2\pi f t + \pi \dot{f} t^2), \quad (11)$$

where $A_0 = \frac{M_c}{D_L} (\pi \mathcal{M}_c f)^{2/3}$ is the amplitude of the signal, $\mathcal{M}_c = M_{\text{BH}}^3 M_{\text{WD}}^3 / M$ is the chirp mass of the binary, ι is the inclination of the binary with respect to the line of sight, and ϕ_0 is the initial phase. Thus, GW observations provide us A_0 , f , and \dot{f} and we cannot infer the individual masses without further assumptions. In order to assess how the universal relations we derived can be combined with LISA measurements, we consider an accreting WDBH system at two different stages of its evolution:

1. “high frequency” (HF): $M_{\text{BH}} = 7.02 M_{\odot}$, $M_{\text{WD}} = 0.10 M_{\odot}$,
 $f = 5 \text{ mHz}$, $\dot{f} = -3.8 \times 10^{-16} \text{ Hz s}^{-1}$;
2. “low frequency” (LF): $M_{\text{BH}} = 7.02 M_{\odot}$, $M_{\text{WD}} = 0.06 M_{\odot}$,
 $f = 3 \text{ mHz}$, $\dot{f} = -3.2 \times 10^{-17} \text{ Hz s}^{-1}$;

We compute LISA’s response following Cornish & Littenberg (2007) and Robson & Cornish (2017) to generate mock data and perform a full Bayesian analysis to infer the posterior distribution of the parameters of the source. For the noise level, we use the SciRdv1 curve (LISA Science Study Team 2018) including a confusion noise due to the galactic foreground in addition to the instrument noise Mangiagli et al. (2020). The parameter estimation is performed with the nested sampling algorithm Multinest (Feroz et al. 2009). We assume a mission duration of 6 yr and two values of the duty cycle: 100% and 75%. We set the distance to $D_L = 10 \text{ kpc}$ and simulate the effect of a reduced duty cycle by placing the source further. For almost monochromatic sources, the angles essentially affect the signal-to-noise ratio (S/N) and have little impact on our analysis. For a duty cycle of 100%, the HF and LF systems have S/Ns of 91 and 26, respectively. Systems at frequencies below 3 mHz, although more numerous, have little chance of being detected due to the galactic foreground. With a duty cycle of 75%, f and \dot{f} are measured within $5 \times 10^{-7} \text{ Hz}$ and $5 \times 10^{-18} \text{ Hz s}^{-1}$ for the HF system and an order of magnitude worse for the LF system.

In Table 1 we report the estimates of the binary masses (normalized to the injected values) directly using the fits to the evolutionary tracks of Figure 2. We can use these results to infer the chirp mass and, from the measurement of A_0 , the distance to the source. We find a reasonable agreement with the injected values (within 5%). However, for the HF system, the injected values lie outside the 90% confidence intervals. This is because the systematics of the model dominate over the statistical uncertainty. In particular, the very narrow range for M_{WD} is due to the extremely good measurement of f . To correct for this, we estimate numerically the values of α_1 and α_2 that best align the evolutionary tracks, $M_{\text{WD}} M_{\text{BH}}^{-\alpha_1}$ and $\dot{f} M_{\text{BH}}^{-2/3 - \alpha_2}$ as functions of f . The exponents α_1 and α_2 are frequency dependent and are determined for each system in the frequency range of observation. We then convolve LISA posteriors with the aligned tracks to infer M_{BH} and M_{WD} .

In Figure 3, we show how the measurement of f and \dot{f} together with this procedure translates into a measurement of the WD and BH masses for the two systems assuming a 75% duty

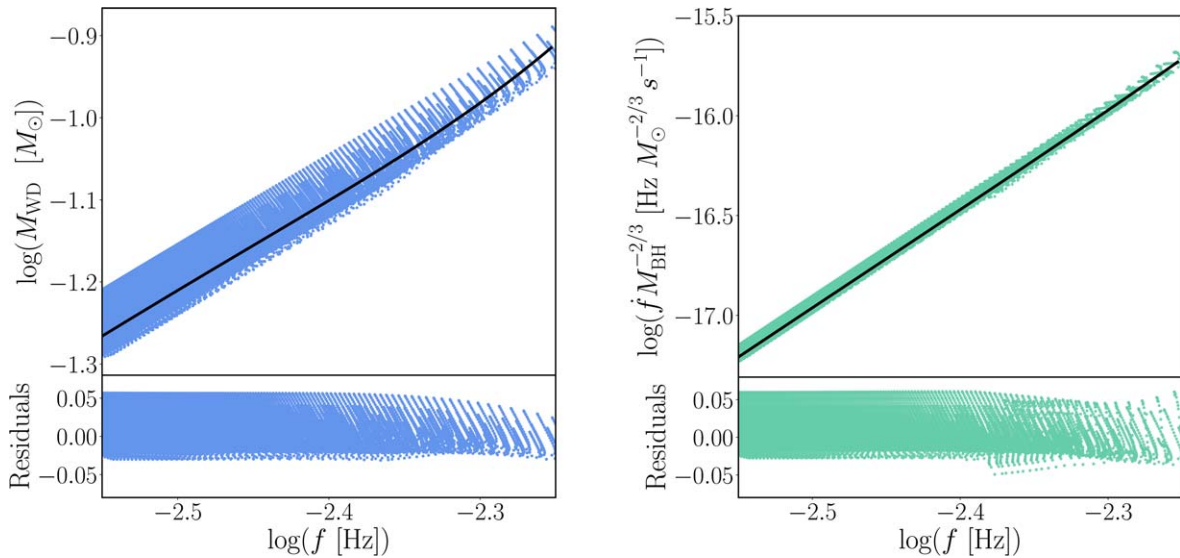


Figure 2. Evolutionary tracks of 400 WDBH binaries and their polynomial fits (black line). We focus on frequencies relevant to LISA.

Table 1

Uncertainties on Individual Masses and Distances Normalized to the Injected Values, Obtained with the Fit to the Global Evolutionary Tracks Relations (Fit) and with the Full Results of Numerical Simulations (Full)

		HF			LF		
		\tilde{M}_{BH}	\tilde{M}_{WD}	\tilde{D}_L	\tilde{M}_{BH}	\tilde{M}_{WD}	\tilde{D}_L
100%	Fit	$0.99^{+0.01}_{-0.01}$	$0.99^{+5.7 \times 10^{-8}}_{-5.8 \times 10^{-8}}$	$1.05^{+0.11}_{-0.14}$	$1.04^{+0.40}_{-0.36}$	$0.97^{+3.8 \times 10^{-7}}_{-2.8 \times 10^{-7}}$	$0.98^{+0.35}_{-0.29}$
	Full	$1.01^{+0.08}_{-0.04}$	$0.99^{+0.02}_{-0.04}$	$1.06^{+0.11}_{-0.15}$	$1.03 + 0.44_{-0.38}$	$0.98^{+0.04}_{-0.05}$	$0.98^{+0.35}_{-0.29}$
75%	Fit	$0.99^{+0.01}_{-0.01}$	$0.99^{+7.7 \times 10^{-8}}_{-7.8 \times 10^{-8}}$	$1.39^{+0.16}_{-0.20}$	$1.05^{+0.55}_{-0.47}$	$0.97^{+3.8 \times 10^{-7}}_{-3.8 \times 10^{-7}}$	$1.28^{+0.59}_{-0.47}$
	Full	$1.01^{+0.08}_{-0.04}$	$0.99^{+0.02}_{-0.04}$	$1.05^{+0.13}_{-0.16}$	$1.03^{+0.61}_{-0.49}$	$0.98^{+0.05}_{-0.05}$	$0.96^{+0.44}_{-0.35}$

Note. The GW frequency f and \dot{f} are measured within 5×10^{-7} Hz and 5×10^{-18} Hz s⁻¹ for the HF system, assuming a duty cycle of 75%. These measurements are an order of magnitude worse for the LF system.

cycle. Table 1 also shows the improvement as compared to fit-based measurements and the very good agreement between the injected and the inferred values obtained with this procedure. M_{BH} is less well constrained than M_{WD} because it relies on the measurement of \dot{f} . The measurement is worse for the LF system due to the lower value of \dot{f} , which results in it not being measured as well during the 6 yr mission. We note that the results are less affected by a reduced duty cycle. Finally, even in the worst scenario the uncertainty on M_{BH} is sufficiently small to unambiguously identify the accretor as a BH.

5. Conclusion

Mass-transferring binaries containing a BH and a WD have been an elusive target, despite being predicted by population synthesis models. In this work we show that combining LISA observations with semianalytic evolution models provides an estimate of the masses of both binary components as well as the distance to the source, which is information not usually accessible from galactic binary GW observations.

WDBH binaries are potential sources of electromagnetic radiation, in particular X-ray emission. The HF and LF systems considered in this work would have, respectively, X-ray luminosity of 9×10^{38} erg s⁻¹ and 1×10^{38} erg s⁻¹ for radiative efficiency of 0.1, well within the capabilities of current

facilities. The fact that we have yet to convincingly identify WDBH binaries among X-ray sources could be explained by the lower rates of these systems, and the difficulty to classify the binary components from electromagnetic emission alone. GW observations such as the ones described in this work, on the other hand, could unequivocally identify the BH companion. The very good localization of the source by LISA, $\mathcal{O}(1 \text{ deg}^2)$, could then provide the opportunity to observe an electromagnetic counterpart. In future work, we will explore the potential synergy between LISA and future electromagnetic surveys (Athena+, Square Kilometer Array) and the detectability of both GW and electromagnetic emission in the Milky Way and nearby galaxies.

To detect and learn the most from these systems with LISA, more detailed modeling will be crucial. This work did not take into account, for instance, the potentially disruptive effect of accretion winds on the accretion stream itself, and its potential variability on short timescales. Moreover, the use of Eggleton's approximation for the Roche lobe radius, which was derived for stars made of incompressible fluids, could introduce a bias in our result. Such bias is hard to quantify because the true relation is unknown. However, our methodology is robust to changes in the Roche lobe radius relation, and we expect our main finding to hold, i.e., LISA could be the first observatory to unambiguously identify WDBH binaries.

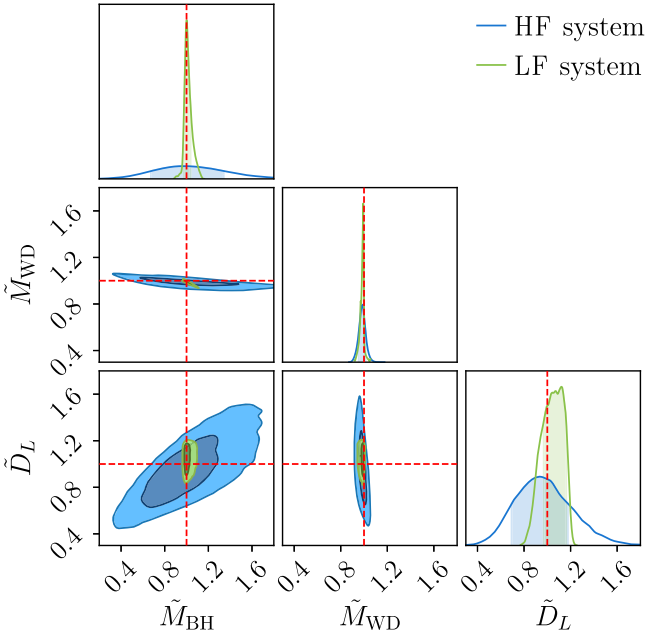


Figure 3. Posterior distributions for binary masses and luminosity distance normalized to the injected values for the high and low frequency systems, at 75% duty cycle. The contours indicate the 50% and 90% confidence intervals and the dashed lines represent the true values (equal to 1 in our normalization). Posteriors are obtained with the rescaled universal relations, as described in Section 4.

Assuming a simple blackbody law for the BH and the WD, we estimate that emission from the BH disk could heat up the WD to $\mathcal{O}(10^5)$ K. Such low temperatures, if interpreted as core temperatures, have very little impact on the mass–radius relation (Bédard et al. 2020) and therefore the cold WD assumption remains a good approximation. A caveat is that the results of Bédard et al. (2020) were obtained for cooling sequences of isolated WDs. More simulations of heated WDs as in Piro et al. (2005) could provide further insight on the effect of illumination on the evolution of WDBH binaries. WDs with masses lower than the ones considered in this work might also exhibit a stronger dependence on the temperature, see, e.g., Deloye & Bildsten (2003). Recent hydrodynamical simulations (Church et al. 2017) have suggested that mass transfer in WDBH binaries could be unstable above WD masses $0.2 M_{\odot}$, leading the binary to merge. It would be interesting to extend our model to lighter WDs, in a mass range where finite temperature effects might become relevant.

Finally, we checked that the presence of tidal torques would not affect our results significantly for small synchronization timescales ($\tau \lesssim 100$ yr). This study could therefore apply to broader classes of galactic binaries.

We are grateful to Katelyn Breivik and Gijs Nelemans for constructive suggestions. A.T. is thankful to Stas Babak and Enrico Barausse for fruitful discussion and their support during the preparation of this work. M.C.M. thanks the Radboud Excellence Initiative for supporting his stay at Radboud University during part of this work. M.C.M. and A.T. are grateful for the hospitality of Perimeter Institute where part of this work was carried out. Research at Perimeter Institute is supported in part by the Government of Canada through the Department of Innovation, Science and Economic Development Canada, and by the Province of Ontario through the Ministry of Colleges and Universities. A.T. was supported by

the European Union’s Horizon 2020 research and innovation program under the Marie Skłodowska-Curie grant agreement No. 690904. A.T. also acknowledges networking support from the COST Action CA16104.

Appendix A Separation Equation

The equation for the orbital separation of the binary can be derived from Equations (4), (5) and (6) and reads

$$\begin{aligned} \frac{\dot{a}}{2a} = & -\frac{1}{1 - 3(1+q)kr_2^2} \left[\frac{j_{\text{GW}}}{J_{\text{orb}}} + \left(1 - \frac{q}{2(1+q)} \right. \right. \\ & + \frac{1}{2}qkr_2^2 + (1+q)\lambda kr_2^2 \left. \left. \frac{\dot{M}_{\text{WD}}}{M_{\text{WD}}} \right. \right. \\ & + \left. \left. \left(q - \frac{q}{2(1+q)} + \frac{1}{2}qkr_2^2 + j_{\text{GR}} \sqrt{(1+q)r_{\text{ISCO}}} \right) \right. \right. \\ & \left. \left. \times \frac{\dot{M}_{\text{BH}}}{M_{\text{WD}}} \right], \end{aligned} \quad (\text{A1})$$

where $r_i = R_i/a$.

Appendix B Equilibrium Solutions

After the initial phase of mass accretion, a very good approximation of the mass transfer rate can be obtained by setting the rhs of Equation (7) to 0 (Marsh et al. 2004) and $\dot{M}_{\text{BH}} = -\epsilon_{\text{ISCO}}\dot{M}_{\text{WD}}$. We find

$$\frac{\dot{M}_{\text{WD,e}}}{M_{\text{WD}}} = -\frac{j_{\text{GW}}/J_{\text{orb}}}{K_{\text{eq}}}, \quad (\text{B1})$$

where

$$\begin{aligned} K_{\text{eq}} = & \frac{\zeta_{\text{WD}} - \zeta_{r_L}}{2} (1 - 3(1+q)kr_{\text{WD}}^2) + (1+q) \\ & \times \lambda kr_{\text{WD}}^2 (1 - \epsilon_{\text{ISCO}}) \left(\frac{1}{2}qkr_{\text{WD}}^2 - \frac{q}{2(1+q)} \right) + 1 \\ & - \epsilon_{\text{ISCO}} (q + j_{\text{GR}} \sqrt{(1+q)r_{\text{ISCO}}}). \end{aligned} \quad (\text{B2})$$

Using Kepler’s law, $\frac{\dot{f}}{2f} = -\frac{3\dot{a}}{2a}$ and replacing Equation (B1) in Equation (A1) gives, at equilibrium:

$$\begin{aligned} \frac{\dot{f}}{2f} = & \frac{3j_{\text{GW}}/J_{\text{orb}}}{K_{\text{eq}}(1 - 3(1+q)kr_2^2)} \\ & \times \left[1 + \left(q - \frac{q}{2(1+q)} + \frac{1}{2}qkr_2^2 \right) \right. \\ & + j_{\text{GR}} \sqrt{(1+q)r_{\text{ISCO}}} \times \epsilon_{\text{ISCO}} \\ & \left. - \left(1 + \frac{q}{2(1+q)} + \frac{1}{2}qkr_2^2 + (1+q)\lambda kr_2^2 \right) \right]. \end{aligned} \quad (\text{B3})$$

Table 2
Coefficients for the Fits in Figure 2

	a_0	a_1	a_2	a_3	a_4
$y = M_{\text{WD}} (M_{\odot})$	319.7593186	509.0101135	303.8011829	80.7077869	8.0347503
$y = \dot{f} M_{\text{BH}}^{-2/3} (\text{Hz } M_{\odot}^{-2/3} \text{s}^{-1})$	142.6384491	236.4026829	136.2183828	35.5719325	3.4778346

Furthermore,




$$\frac{\dot{J}_{\text{GW}}}{J_{\text{orb}}} = \frac{32 G^3 M_{\text{BH}} M_{\text{WD}} M}{5 c^5 a^4} \propto M_{\text{BH}} M_{\text{WD}} M \left(\frac{M}{f^2} \right)^{4/3} \simeq M_{\text{BH}}^{2/3} M_{\text{WD}} f^{8/3}. \quad (\text{B4})$$

where in the last step we used $M_{\text{WD}} \ll M_{\text{BH}}$, so that $M \simeq M_{\text{BH}}$. Finally, the late time evolution of the other terms in Equation (B3) happens to have a weak dependence on M_{BH} , so $\dot{f} M_{\text{BH}}^{-2/3}$ is an almost M_{BH} independent quantity as verified in Figure 2, right panel.

Appendix C Fits to the Evolutionary Tracks

The coefficients for the evolutionary track fits described in the main text are summarized in Table 2.

ORCID iDs

Laura Sberna  <https://orcid.org/0000-0002-8751-9889>
 Alexandre Toubiana  <https://orcid.org/0000-0002-2685-1538>
 M. Coleman Miller  <https://orcid.org/0000-0002-2666-728X>

References

- Adams, M. R., Cornish, N. J., & Littenberg, T. B. 2012, *PhRvD*, **86**, 124032
 Amaro-Seoane, P., Audley, H., Babak, S., et al. 2017, arXiv:1702.00786
 Bédard, A., Bergeron, P., Brassard, P., & Fontaine, G. 2020, *ApJ*, **901**, 93
 Breivik, K., Coughlin, S., Zevin, M., et al. 2020b, *ApJ*, **898**, 71
 Breivik, K., Kremer, K., Bueno, M., et al. 2018, *ApJL*, **854**, L1
 Breivik, K., Mingarelli, C. M., & Larson, S. L. 2020a, *ApJ*, **901**, 4
 Campbell, C. G. 1984, *MNRAS*, **207**, 433
 Chandrasekhar, S. 1984, in *General Relativity and Gravitation*, ed. B. Bertotti, F. de Felice, & A. Pascolini (Dordrecht: D. Reidel), 5
 Church, R. P., Strader, J., Davies, M. B., & Bobrick, A. 2017, *ApJL*, **851**, L4
 Cornish, N. J., & Littenberg, T. B. 2007, *PhRvD*, **76**, 083006
 Deloye, C. J., & Bildsten, L. 2003, *ApJ*, **598**, 1217
 Dong, Y.-Z., Gu, W.-M., Liu, T., & Wang, J. 2018, *MNRAS*, **475**, L101
 Eggleton, P. P. 1983, *ApJ*, **268**, 368
 Feroz, F., Hobson, M., & Bridges, M. 2009, *MNRAS*, **398**, 1601
 Fuller, J., & Lai, D. 2012, *MNRAS*, **421**, 426
 Hurley, J. R., Tout, C. A., & Pols, O. R. 2002, *MNRAS*, **329**, 897
 Korol, V., Rossi, E. M., & Barausse, E. 2018, *MNRAS*, **483**, 5518
 Korol, V., Rossi, E. M., Groot, P. J., et al. 2017, *MNRAS*, **470**, 1894
 Korol, V., Toonen, S., Klein, A., et al. 2020, *A&A*, **638**, A153
 Kremer, K., Breivik, K., Larson, S. L., & Kalogera, V. 2017, *ApJ*, **846**, 95
 Kremer, K., Chatterjee, S., Breivik, K., et al. 2018, *PhRvL*, **120**, 191103
 Lamberts, A., Blunt, S., Littenberg, T. B., et al. 2019, *MNRAS*, **490**, 5888
 Lamberts, A., Garrison-Kimmel, S., Hopkins, P. F., et al. 2018, *MNRAS*, **480**, 2704
 LISA Science Study Team 2018, LISA Science Requirements Document, <https://www.cosmos.esa.int/documents/678316/1700384/SciRD.pdf/25831f6b-3c01-e215-5916-4ac6e4b306fb?t=1526479841000>
 Littenberg, T. B., & Yunes, N. 2019, *CQGra*, **36**, 095017
 Liu, J., Han, Z., Zhang, F., & Zhang, Y. 2010, *ApJ*, **719**, 1546
 Maccarone, T. J., Kundu, A., Zepf, S. E., & Rhode, K. L. 2007, *Natur*, **445**, 183
 Mangiagli, A., Klein, A., Bonetti, M., et al. 2020, *PhRvD*, **102**, 084056
 Marsh, T. R., Nelemans, G., & Steeghs, D. 2004, *MNRAS*, **350**, 113
 Miller-Jones, J. C. A., Strader, J., Heinke, C. O., et al. 2015, *MNRAS*, **453**, 3918
 Nelemans, G. 2005, in *ASP Conf. Ser.*, 330, *The Astrophysics of Cataclysmic Variables and Related Objects*, ed. J. M. Hameury & J. P. Lasota (San Francisco, CA: ASP), 27
 Nelemans, G., Portegies Zwart, S. F., Verbunt, F., & Yungelson, L. R. 2001a, *A&A*, **368**, 939
 Nelemans, G., Yungelson, L., & Portegies Zwart, S. 2004, *MNRAS*, **349**, 181
 Nelemans, G., Yungelson, L. R., & Portegies Zwart, S. F. 2001b, *A&A*, **375**, 890
 Nelemans, G., Yungelson, L. R., Portegies Zwart, S. F., & Verbunt, F. 2001c, *A&A*, **365**, 491
 Piro, A. L., Arras, P., & Bildsten, L. 2005, *ApJ*, **628**, 401
 Robson, T., & Cornish, N. 2017, *CQGra*, **34**, 244002
 Roebber, E., Buscicchio, R., Vecchio, A., et al. 2020, *ApJL*, **894**, L15
 Ruiter, A. J., Belczynski, K., Benacquista, M., Larson, S. L., & Williams, G. 2010, *ApJ*, **717**, 1006
 Shah, S., Larson, S. L., & Brown, W. 2015, *JPhCS*, **610**, 012003
 Toonen, S., Claeys, J. S. W., Mennekens, N., & Ruiter, A. J. 2014, *A&A*, **562**, A14
 Tudor, V., Miller-Jones, J. C. A., Knigge, C., et al. 2018, *MNRAS*, **476**, 1889
 van Haften, L. M., Nelemans, G., Voss, R., Wood, M. A., & Kuijpers, J. 2012, *A&A*, **537**, A104
 Verbunt, F., & Rappaport, S. 1988, *ApJ*, **332**, 193
 Webbink, R. F. 1984, *ApJ*, **277**, 355
 Yu, S., & Jeffery, C. S. 2010, *A&A*, **521**, A85
 Yungelson, L. R., Lasota, J.-P., Nelemans, G., et al. 2006, *A&A*, **454**, 559
 Zahn, J. P. 1977, *A&A*, **500**, 121